Increasing the Conversion Efficiency of Dye-Sensitized TiO_2 Photoelectrochemical Cells by Coupling to Photonic Crystals

Lara I. Halaoui,*,†,‡ Neal M. Abrams,† and Thomas E. Mallouk*,†

Department of Chemistry and Center for Nanoscale Science, The Pennsylvania State University, University Park, Pennsylvania 16802, and Chemistry Department, American University of Beirut, Beirut, 110236 Lebanon

Received: December 19, 2004

The mechanism of enhancing the light harvesting efficiency of dye-sensitized TiO_2 solar cells by coupling TiO_2 inverse opals or disordered scattering layers to conventional nanocrystalline TiO_2 films has been investigated. Monochromatic incident photon-to-current conversion efficiency (IPCE) at dye-sensitized TiO_2 inverse opals of varying stop band wavelengths and at disordered titania films was compared to the IPCE at bilayers of these structures coupled to nanocrystalline TiO_2 films and to the IPCE at nanocrystalline TiO_2 electrodes. The results showed that the bilayer architecture, rather than enhanced light harvesting within the inverse opal structures, is responsible for the bulk of the gain in IPCE. Several mechanisms of light interaction in these structures, including localization of heavy photons near the edges of a photonic gap, Bragg diffraction in the periodic lattice, and multiple scattering events at disordered regions in the photonic crystal or at disordered films, lead ultimately to enhanced backscattering. This largely accounts for the enhanced light conversion efficiency in the red spectral range (600−750 nm), where the sensitizer is a poor absorber.

I. Introduction

Significant research effort has been dedicated in recent years to the study of dye-sensitized semiconducting particles and electrodes. The pioneering example of the dye-sensitized nanocrystalline TiO_2 solar cell by Grätzel and co-workers in the early 1990s,[1−3] with its low-cost and compact structure, has spurred an increasing interest in nanostructured photoelectrodes as an alternative to conventional single-crystal solar cells. In this cell, an optically excited dye injects electrons into the conduction band of a nanocrystalline titanium dioxide film, which transports the photogenerated carriers to the back-contact.[1−5] A triiodide/iodide redox couple provides the transport pathway for the hole from the oxidized dye molecule to the counter electrode, thus completing the redox cycle. The incident photon-to-current conversion efficiency (IPCE) is determined by the sensitizer light-harvesting efficiency, the quantum yield for electron injection from the excited dye to the conduction band of the semiconductor, and the collection efficiency of the electron at the back-contact.[4] Recombination of photogenerated electrons through back-transfer from TiO_2 to the redox species ($I_3^- + 2e \rightarrow 3I^-$) resulting in an open-circuit photovoltage lower than the theoretical maximum,[2,5,6] together with thermal energy losses in the I^-/I_3^- redox cycle and the low extinction coefficient of the $RuL_2(SCN)_2$ (L = 2,2′-bipyridyl-4,4′-dicarboxylic acid) dyes in the red and infrared, have constituted major limitations to the performance of this cell.

Development of photosensitizers with improved spectral response[7] at the low energy of the solar spectrum has not proven successful because dye molecules with high red absorbance have lower excited-state excess free energy, thus lowering the quantum yield for charge injection. Increasing the thickness of the film beyond 10−12 μm in order to increase the absorbance in the red results in an increase in the electron transport length and the recombination rate, thereby decreasing the photocurrent. An alternative approach to improving efficiency is to increase the path length of light by enhancing light scattering in the TiO_2 films.[8,9] While the small size of TiO_2 nanoparticles (10−30 nm) employed to ensure a high surface area makes conventional nanocrystalline TiO_2 films poor light-scatterers,[9,10] mixing the nanoparticles with larger particles[9] or applying a scattering layer[8,9,11] to the nanocrystalline film has been shown in simulations and some experimental studies to increase light-harvesting by enhancing the scattering of light.

Recently, we experimentally reported an enhancement in the light conversion efficiency of $RuL_2(SCN)_2$-sensitized TiO_2 solar cells by coupling a conventional nanocrystalline TiO_2 film to a TiO_2 inverse opal with a stop band centered at 610 nm (as measured in ethanol).[12] When illuminated from the electrolyte side of the TiO_2 film (hereinafter referred to as front-wall illumination), this bilayer resulted in a 26% increase in the IPCE relative to a nanocrystalline film of the same overall thickness, in the 550−800 nm spectral range. The improved conversion efficiency was thought to arise from localization of heavy photons at the edges of the photonic stop band,[12−15] and from Bragg diffraction and scattering within the photonic crystal (PC),[16] but the contributions of these different mechanisms were not quantified. An increased absorbance was found for dye adsorbed on titania inverse-opals at energies to the red edge of the stop-band. This phenomenon, which has also been observed by Asher et al. in silver silica colloidal crystals,[17] is attributed to the slowing of the group velocity of light near the edges of a photonic gap.[13]-15 The observation of increased red absorbance suggested that photon localization was the primary reason for the increase in IPCE.

The mechanism of enhancement in solar energy conversion in structures where a degree of light localization is in effect is

* Corresponding authors. E-mail: lh07@aub.edu.lb. E-mail: tom@chem.psu.edu.

† The Pennsylvania State University.

‡ American University of Beirut.

10.1021/jp044228a CCC: $30.25
Published on Web 03/11/2005

further explored in this work. Monochromatic IPCE measurements at dye-sensitized TiO_2 inverse opals of varying stop band wavelengths were compared to IPCE at bilayers of inverse opal/nano-TiO_2 films and at nano-TiO_2 films. The mechanism of light propagation and the resulting extent of localization and hence the cell conversion efficiency were found to depend on both order and disorder in the photonic crystals. In addition to Bragg reflection by the ordered lattice, localization of heavy photons at the edges of the photonic gap and, particularly, multiple internal scattering events at disordered regions ultimately leading to enhanced backscattering appear to explain the increased IPCE at inverse opal/nano-TiO_2 bilayer photoelectrodes. Similar improvement in the long-wavelength spectral region was also achieved by coupling disordered titania films to a conventional nanocrystalline TiO_2 layer. This improvement is believed to result from multiple scattering events in the disordered films, possibly leading to weak localization of light.

II. Experimental Methods

Materials. Suspensions of monodisperse carboxylate-modified polystyrene spheres ($\langle d \rangle = 150$ or 243 nm; $\sigma = 2\%$; 30.35 wt % in water) were purchased from Seradyn Co., stored at 4 °C and used without further purification. Ammonium hexafluorotitanate ($(NH_4)_2TiF_6$, 99.99%, Aldrich), titanium isopropoxide (Aldrich), boric acid (H_3BO_3, 99.5% Aldrich), polyoxyethylene(5)nonyl phenyl ether (Igepal CO-520, Aldrich), TiO_2 nanoparticles slurry (Ti−nanoxide; $\langle d \rangle = 13$ nm; Solaronix), *cis*-bis(isothiocyanato)bis(2,2′-bipyridyl-4,4′-dicarboxylato)ruthenium(II) bis(tetrabutylammonium) ($RuL_2(NCS)_2$−2TBA also known as Ruthenium535 bis-TBA, or N719, Solaronix), and 200 proof ethanol were used as purchased. The TiO_2 nanoparticle slurry was either purchased (Ti−nanoxide; $\langle d \rangle = 13$ nm; Solaronix) or synthesized according to published procedures.[18] The redox couple/electrolyte solution consisted of iodide/triiodide solution (Iodolyte TG50, Solaronix). Electrodes were fluorine-doped tin oxide coated glass substrates (F:SnO_2 or FTO, TEC8, Hartford Glass Co., IN). All aqueous solutions were prepared with deionized ultrapure water of resistivity ≥ 18.3 MΩ·cm.

Preparation of TiO_2 Photonic Crystals. TiO_2 inverse opal films were prepared on FTO substrates by replication of a polystyrene colloidal crystal template according to a previously reported liquid-phase deposition (LPD) method.[12,19,20] Substrates were cleaned by sonication for 10 min in deionized water and for 30 min in 2-propanol in an ultrasonic bath, followed by rinsing with water and drying in air. Colloidal crystals were prepared following a modification of the method of Jiang et al.[21] Monodisperse carboxylate-modified polystyrene (PS) suspensions in water were sonicated for 30 min to break down aggregated particles, and Igepal (0.003 wt %) was added to minimize agglomeration. The synthetic opal templates were assembled by immersing substrates vertically in the PS suspensions and evaporating the solvent at 55 °C. A 0.1 wt % PS suspension in water resulted in a 6 μm thick colloidal crystal. Thinner films could be prepared by starting with lower PS concentrations in proportion to the desired thickness.

In the LPD growth of TiO_2, the colloidal crystal was immersed in a solution of 1.2% (w/v) of titanium isopropoxide and 0.12% HNO_3 in ethanol followed by hydrolysis for 5 min in air to form a titania surface seed layer. The crystals were then vertically submerged for 30 min in an aqueous solution of 0.20 M ammonium hexafluorotitanate and 0.25 M boric acid held at 51 ± 2 °C. The pH of the solution was first adjusted to 2.8−3.0 with 1 M HCl. After 30 min the samples were rinsed thoroughly with deionized water and dried in air at room temperature. The latex spheres were removed by calcination in air at 400 °C for 8 h, leaving behind an inverse opal anatase TiO_2 structure.

The position of the stop band was tuned by subjecting the inverse opals to a second LPD step, by immersion in 0.20 M $(NH_4)_2TiF_6$/0.25 M H_3BO_3(aq) solution at pH 2.8−3.0 held at 51 ± 2 °C. The thickness of the walls was controlled by varying the deposition time,[19] at a rate resulting in a 4.4 nm red shift in the stop band per minute of reaction time. Reported stop bands are for samples immersed in ethanol, unless otherwise indicated.

Preparation of Disordered Structures. Disordered films of titanium dioxide were grown by filling the voids of a disordered template of latex spheres by the same LPD protocol as described above, with calcination of the latex spheres in air at 400 °C for 8 h. Disordered templates were assembled on F:SnO_2 glass by evaporating (sonicated) 0.08 wt % suspensions of polystyrene spheres of 243 nm diameter mixed with 150 nm diameter spheres in a 2/1 ratio, at 55 °C under ambient. Igepal was similarly added to the suspension at 0.003 wt % prior to sonication (30 min). To vary the void fraction, the titania films thus prepared were subjected to a second LPD for 30 min by the same procedure, after calcination of the latex spheres. These films are termed disordered TiO_2_2 in reference to the second LPD step.

Electrode Assembly. A film of TiO_2 nanoparticles was applied to the surface of the TiO_2 inverse opal, TiO_2 disordered film, or an FTO electrode by means of a squeegee method to give a total film thickness of 10−11 μm. Cellophane tape was used as a spacer to control the film thickness. The solvent was dried at 80 °C for 10 min, and the nanoparticles were sintered at 400 °C for 1 h and cooled to room temperature. Prior to dye sensitization, titania films were dehydrated at 120 °C for 1 h. Films were immersed at this temperature in a 0.3 mM solution of N719 dye in dry ethanol for 48 h. Sensitized electrodes were stored in dry ethanol in the dark. The amount of dye adsorbed onto the different structures was determined spectrophotometrically (by UV−vis absorption) after desorption in 3.8 M NaOH solution to be as follows: 132 nmol/cm^2 on a 10−11 μm nano-TiO_2 film, 19 nmol/cm^2 on a 6 μm inverse opal (stop band at 488 nm), 28 nmol/cm^2 on a 6 μm inverse opal (stop band at 582 nm), 37 nmol/cm^2 on the disordered 4.5 μm titania film, and 38 nmol/cm^2 on a 4.5 μm disordered TiO_2_2 film.

The cell was assembled by sandwiching a 50 μm thick PET spacer between the dye-sensitized photoelectrode and an FTO counter electrode and pressing the assembly with a binder clip. The two electrodes were placed in a glass cuvette (Starna Cells, CA) containing a small volume of electrolyte, and the solution filled the space between the electrodes by capillary action.

Photoelectrochemical Measurements. Photocurrent measurements were made in a three-electrode configuration using a Ag/AgCl reference electrode, by scanning between −5 and +5 mV at 1 mV/s. Photoelectrodes were irradiated from a Xe lamp operated at 140 W (Oriel instruments, 6256, 150 W) and equipped with a monochromator (Oriel instruments, Model 77250); either in front-wall (through the electrolyte) or back-wall (through the TiO_2 electrode) illumination modes. Photocurrents were measured using a BAS electrochemical workstation (Bioanalytical Systems, BAS-100B/W), and short-circuit photocurrents (I_{sc}) are reported after subtraction of dark currents. The lamp spectrum was acquired using a thermopile light detector (Ophir Optronics, thermal surface absorbing head 2A-SH with NOVA display) with 10 s average light measurements.

Characterization. UV−visible absorption and transmission spectra were collected using a diode array spectrophotometer (Hewlett-Packard, HP8452A). Absorption spectra of films on FTO were measured against the FTO substrate as a blank. Scanning electron micrographs were collected using a JEOL JSM5400 or JEOL 6700F FESEM microscope operated at 20 or 5 kV, respectively, after sputtering a thin gold film. For thickness measurement, the surface was cut with a sharp surgical blade, and scanning electron microscopy (SEM) images were acquired with tilt angles taken into consideration for the thickness calculation. A profilometer (Tencor Instruments Profilometer, Alpha 3.7-2) was also employed for routine thickness measurements. Powder X-ray diffraction patterns of the TiO_2 inverse opal (scraped off the FTO surface) were acquired using a Philips X-Pert MPD diffractometer (Cu Kα anode, operated at 40 kV, 40 mA) at a scan speed of 0.030° 2θ/s. High-resolution transmission electron microscopy (TEM) images were acquired using a transmission electron microscope (JEOL 2010F) operated at 200 kV with a point-to-point resolution of 1.9 Å. TEM samples were deposited on Lacey carbon on copper grids.

III. Results

SEM imaging of colloidal crystals assembled from 243 nm polystyrene spheres showed the latex particles arranged in an fcc lattice, having undergone shrinkage to 215−217 nm during solvent evaporation (Figure 1a). The film had a stop band in air centered at 520 nm, which corresponds to 217 nm polystyrene particles according to the Bragg equation applied to the close-packed crystal (26% void). Replication of this latex colloidal crystal film with titanium dioxide resulted in the inverse opal structure shown in Figure 1b. The titania inverse opal had a stop band centered at 488 ± 2 nm in ethanol (n = 1.36), and 524 ± 2 nm in toluene (n = 1.50). Powder X-ray diffraction (XRD) showed the TiO_2 to be predominantly in the anatase crystal phase (E_g = 3.2 eV), and HRTEM imaging (cf. Figure 2) showed nanocrystalline domain sizes of the order of 10 nm.

The absorption spectrum of the Ru complex dissolved in ethanol or adsorbed on a nano-TiO_2 film is characterized by two absorption peaks of similar extinction coefficients at λ = 400 and 535 nm (Figure 3). Adsorbing the dye onto a mesoporous titania photonic crystal with a stop band centered at 488 nm results in an enhancement of absorbance at the red edge of the stop band and an attenuation of absorbance at the blue edge. When the position of the stop band was tuned to the red, the same effect was observed.[12] This phenomenon is attributed to the appreciable bending of the photon dispersion curve at the edges of the photonic gap, and therefore the slowing of the group velocity of light (heavy photons) in photonic crystals at wavelengths near the gap.[12-15] At the red edge of the stop band, the standing photon wave, or heavy photon, becomes localized in the high dielectric part of the photonic crystal, and at the blue edge the heavy photon is localized in the low dielectric part.[12] This manifests itself by an increase in the absorbed light intensity by dye molecules localized in the high dielectric part of the structure. The same effect has been reported by Asher et al. to result in increasing the plasmon absorbance of silver nanoparticles embedded in a silica photonic crystal.[17] Vlasov et al. also observed that femtosecond light pulses significantly slow at the photonic band edges of a photonic crystal of 254 nm silica particles; delays as long as 100−150 fs have been reported.[15]

When a dye-sensitized 6 μm thick TiO_2 inverse opal with a 486 nm stop band was coupled to a 5 μm nano-TiO_2 film, the photoaction spectrum exhibited two maxima in accordance with the absorption spectrum of the photosensitizer, but a higher IPCE was observed at the bilayer compared to a 10−11 μm nano-TiO_2 film in both front-wall and back-wall illumination in the 550−800 nm spectral region (cf. Figure 4a,b, i and ii). This is consistent with our previous observation of IPCE enhancement for a photonic crystal (610 nm stop band)/nano-TiO_2 bilayer in front-wall illumination.[12] The low conversion efficiency at 400−450 nm results from attenuation of light by triodide, which absorbs strongly at these wavelengths. The dip in the IPCE of the PC−TiO_2 bilayer at 480−500 nm in backwall illumination is caused by a lower light intensity reaching the nano-TiO_2 layer because of significant Bragg reflection at these wavelengths. Scattering at disordered regions in the photonic crystal and the higher amount of I_3^- in its open structure could account for the lower IPCE at the photonic crystal/TiO_2 bilayer relative to the nanoTiO_2 film at wavelengths shorter than 450 nm in back-wall illumination.

To assess the role of internal light propagation and energy conversion in the photonic crystal itself, the IPCE at the dye-

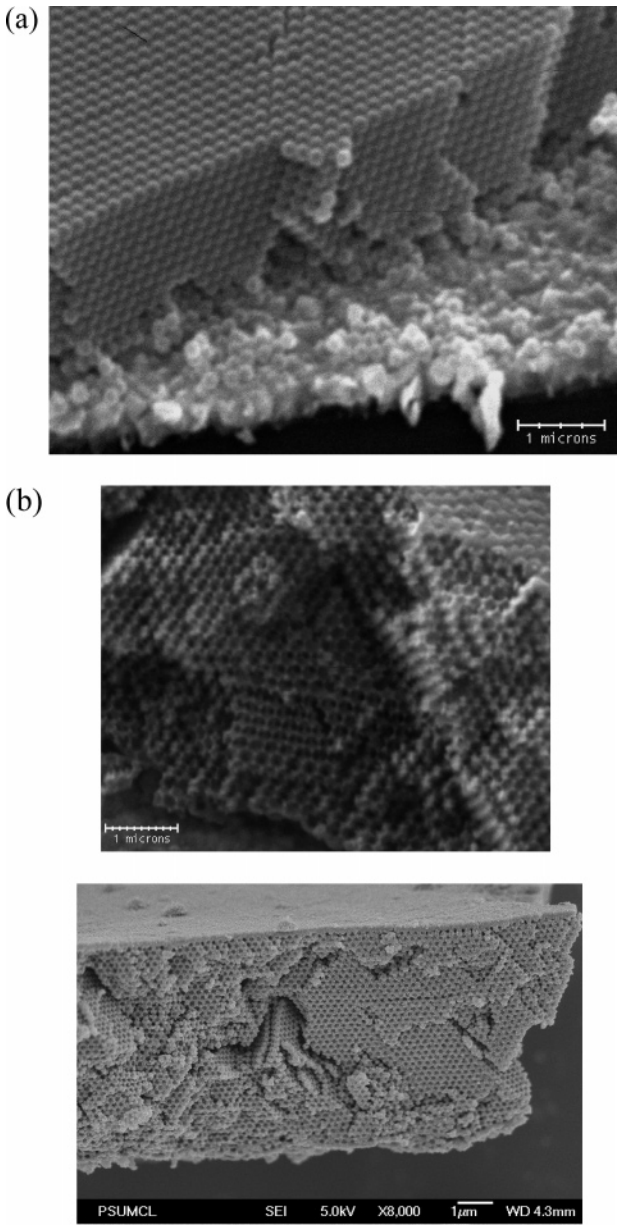

Figure 1. SEM images of a polystyrene (243 nm diameter) photonic crystal (a), and a TiO_2 inverse opal structure (b).

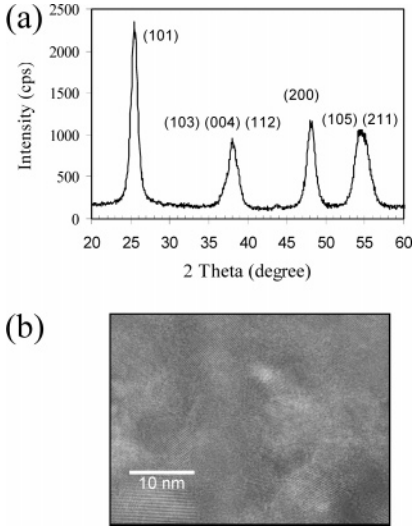

Figure 2. X-ray powder diffraction pattern (a) and the HRTEM image (b) of TiO_2 grown by liquid-phase deposition (LPD) in the voids of the latex colloidal crystal template.

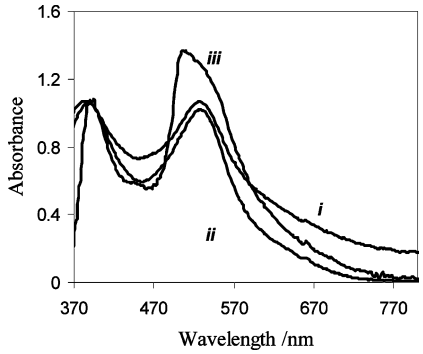

Figure 3. UV−visible absorption spectra of the dye solution in ethanol (i) and the dye adsorbed on a nanocrystalline TiO_2 film (ii) and on a titania inverse opal with stop band centered at 490 nm in ethanol (iii). Spectra are normalized to the absorbance at 400 nm. The spectra in ii and iii were collected after filling the void volume with ethanol (n = 1.36). Absorption spectra of the films before dye adsorption were subtracted from ii and iii.

sensitized TiO_2 inverse opal (stop band at 486 nm) in Figure 4 (iii) was compared to the IPCE of nano-TiO_2 films.[22] The effective surface area of the 6 μm PC was found by dye adsorption measurements to be comparable to that of a 1.4−1.6 μm nanocrystalline TiO_2 film. At the peak wavelength of 540 nm, the short-circuit photocurrent density (J_{sc}) at a 10 μm nano-TiO_2 film was a factor of 2.9 (back-wall) or 2.5 (front-wall) higher than the I_{sc} generated at the photonic crystal. Because of the high extinction coefficient of the photosensitizer at this wavelength, there is an inner filter effect in the nanocrystalline TiO_2 film,[4] causing most of the incident light to be absorbed in the first few micrometers. On the other hand, at 680 nm where the dye has a low extinction coefficient, light is homogeneously absorbed and therefore the short-circuit photocurrent increases in proportion to the nano-TiO_2 film thickness (or surface area).[4]

An enhancement factor (in the conversion efficiency) can be computed for the inverse opal titania structures relative to the nanocrystalline TiO_2 film as the ratio of surface area to IPCE at 680 nm. These results are summarized in Table 1. The monochromatic IPCE at 680 nm at the nanocrystalline film in front-wall illumination was a factor of 7.2 higher than that measured at the inverse opal, which is proportional within experimental error to its seven-times higher surface area. The

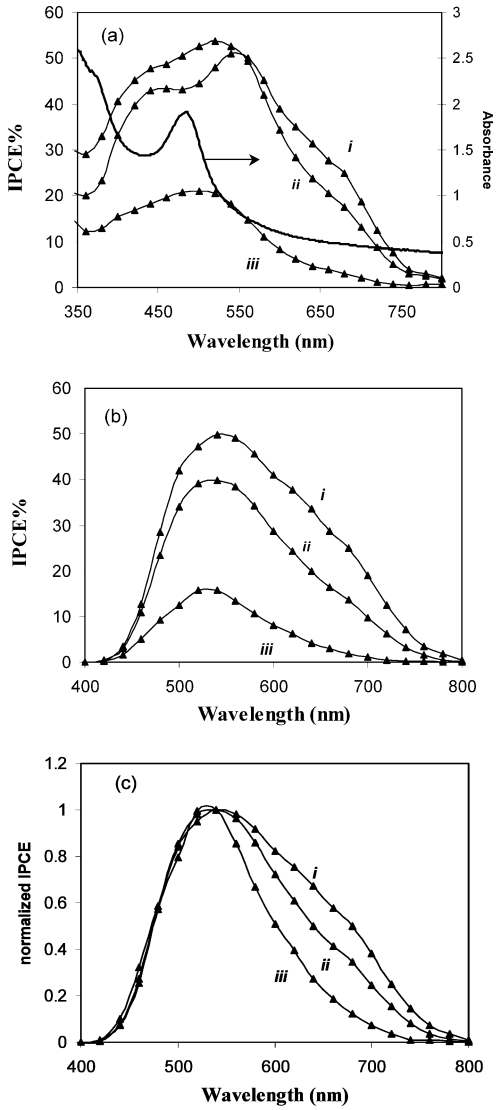

Figure 4. Photoaction spectra in back-wall (a) and front-wall illumination (b) of a dye-sensitized TiO_2 inverse opal/nanocrystalline TiO_2 bilayer (i), a nanocrystalline TiO_2 film (ii), and the TiO_2 inverse opal (iii). Normalized photoaction spectra (front wall) are shown in c. The inverse opal film is 6 μm thick, and the TiO_2 nanocrystalline film and the bilayer structure are 10−11 μm thick. The absorbance spectrum of this photonic crystal with ethanol filling the void is presented (right axis, panel a), showing the stop band centered at 488 ± 2 nm.

linear dependence of IPCE on surface area at this wavelength indicates that this PC is converting light at the same efficiency per molecule of adsorbed dye as a nanocrystalline TiO_2 film, thus showing the absence of enhancement in light harvesting due to internal multiple scattering in the PC in the red spectral range.

The improved light conversion at the bilayer at 550−800 nm is therefore a result of enhanced beam intensity at the nanocrystalline film due to its proximity to the PC, rather than to photon localization in the crystal. The increase in I_{sc} at the photonic crystal/nano-TiO_2 bilayer at 680 nm relative to a nano-TiO_2 electrode was larger than the photocurrent generated at the photonic crystal itself, further supporting this conclusion. The photocurrent at the bilayer was also larger than expected from the contribution of the two layers if uncoupled. The synergistic effect on the light conversion efficiency resulting from the coupled architecture is summarized in Table 2. In this case, the monochromatic IPCE at 680 nm equals 25% at the bilayer in front-wall illumination compared to a mere 1.9% at

TABLE 1: IPCE Ratio at a Nanocrystalline TiO_2 Film and Photonic Crystal (PC) or Disordered Titania Inverse Opal, Compared to the Ratio of Respective Surface Areas, and the Corresponding Enhancement Factor in the Conversion Efficiency in the Red[a,b]

	surface area ratio	IPCE ratio	enhancement factor
TiO_2 to PC (486 nm)	7	7 at 680 nm	1 at 680 nm
TiO_2 to PC (582 nm)	4.8	3.8 at 680 nm	1.3 at 680 nm
		3.3 at 640 nm [c]	1.5 at 640 nm
disordered TiO_2 (LPD1)	3.5	2.3 at 680 nm	1.5 at 680 nm
disordered TiO_2_2 (LPD2)	3.4	1.3 at 680 nm	2.6 at 680 nm

[a] Front-wall illumination. [b] The enhancement factor resulting from the internal localization in the PC or disordered inverse opal film is computed as the surface area ratio to the IPCE ratio. [c] Reported at 640 nm, close to the red edge of this PC stop band (at 582 nm).

TABLE 2: Synergistic Effect at 680 nm from Coupling a PC or a Highly Disordered Titania Inverse Opal Layer to a Nanocrystalline TiO_2 Layer and Overall Gain at the Bilayer Relative to a Nano-TiO_2 Film of the Same Thickness (10−11 μm) at 580−800 nm [a]

	IPCE of PC or disordered, %	IPCE of nano-TiO_2,[b] %	IPCE for bilayer, %	synergistic enhancement, %	gain at 580-800 nm,[c] %
6 μm PC (486 nm)	2	7 (5 μm)	25	16	29
					61
6 μm PC (582 nm)	4	7 (5 μm)	27	16	38
					70
4.5 μm TiO_2 disordered	6	8 (6 μm)	21	7	24
					26
4.5 μm TiO_2 disordered_ 2	12	8 (6 μm)	35	15	71
					83

[a] Front-wall illumination. [b] Computed from a 14−15% IPCE measured at 10 μm TiO_2 film at 680 nm, based on the homogeneous light absorption at this wavelength. [c] First row computed from IPCE data normalized at 540 nm for the bilayer relative to the nanoTiO_2 film of same thickness. Second row (in italics) computed from measured percent IPCE.

the PC. Since the I_{sc} at 680 nm is proportional to the thickness of the nano-TiO_2 film, a 5 μm thick layer would convert 680 nm light with a ∼7% efficiency. This therefore constitutes a 16% enhancement in efficiency at this wavelength that is a direct result of the coupled architecture. It is believed that disorder, originating possibly from template disorder caused by stacking faults and the sphere size distribution and from the chemical infiltration process, causes light scattering at the PC, thus enhancing the beam intensity at the nanocrystalline layer. This is discussed in section IV below.

To elucidate the role that "heavy" photons at the edges of a photonic gap play in determining the light conversion efficiency, the photonic crystal stop band was shifted to 582 nm so it was positioned to the red of maximum dye absorption. Coupling this sensitized 6 μm thick PC to a 5 μm nano-TiO_2 film resulted in a 36% increase in the total conversion efficiency in front-wall illumination relative to a nano-TiO_2 film of the same thickness (Figure 5). The enhancement was predominantly in the spectral region of 580−800 nm (amounting to 94% of the energy gain). In back-wall illumination, however, the total light conversion efficiency at the bilayer was appreciably lower than at the nano-TiO_2 film. This loss is attributed to attenuation of the incident light by scattering and Bragg reflection at the photonic crystal. Nevertheless, a higher IPCE was still achieved at the bilayer at wavelengths to the red of the photonic crystal stop band.

The light conversion efficiency in the red spectral region was higher at this sensitized photonic crystal (stop band at 582 nm) compared to a nano-TiO_2 film of the same surface area; an enhancement factor of 1.3 at 680 nm or 1.5 at 640 nm was measured (cf. Table 1). The monochromatic IPCE at 680 nm at this sensitized inverse opal TiO_2 was only 3.8 times lower (or 3.3 times at 640 nm) than the IPCE at the 10 μm nano-TiO_2 film; which is higher than expected on the basis of its surface area (4.8 times smaller than that of the nano-TiO_2 film). Thus improved light harvesting by the adsorbed dye—due to localization of heavy photons having energies to the red of the 582 nm stop band and internal scattering at disordered regions in the crystal—can account for its somewhat higher conversion efficiency per molecule of adsorbed dye at 600−800 nm.

If light localization in the photonic crystal does not play a major role in enhancing the IPCE, then enhanced scattering in *disordered* TiO_2 structures coupled to nano-TiO_2 films could also improve the light-conversion efficiency of the dye-sensitized cell. To test this hypothesis, disordered templates were assembled from mixtures of different size polystyrene particles (e.g., 150 and 243 nm) and were replicated with TiO_2. An SEM image of the resulting 4.5 μm thick structure is shown in Figure 6, revealing the level of disorder and the nanoparticulate nature of the film. When the cell was operated in front-wall illumination, this disordered titania structure (LPD1) coupled to a nano-TiO_2 layer resulted in a 10% photocurrent gain compared to a nano-TiO_2 film of the same thickness (10 μm), as shown in Figure 7. The gain was mainly measured in the 580−800 nm spectral range, amounting to a 24% higher efficiency relative to the nano-TiO_2 film (Table 2). When operated in back-wall illumination, however, a lower total IPCE resulted at the bilayer, as a result of scattering at the disordered layer, which reduces the intensity of the light reaching the nanocrystalline TiO_2 film. Pronounced scattering at the disordered structure compared to the transparent nano-TiO_2 film was further evidenced by UV−visible transmission spectra in ethanol, shown in Figure 8. Despite the lower efficiency in back-wall illumination, an improvement in IPCE was still measured at the bilayer electrode in the 600−800 nm spectral range.

An enhancement factor of 1.5 in the conversion efficiency at 680 nm resulted at this disordered film relative to a nano-TiO_2 film of the same surface area, which is attributed to multiple internal scattering in the disordered film. The longer path length of light in the disordered structure however cannot account for the entire energy gain at the bilayer electrode. For example, the IPCE at 680 nm at the 4.5 μm disordered titania (equivalent to 2.8−3.1 μm thick nano-TiO_2) in front-wall illumination equaled 6%. Therefore, based on an estimated 8% conversion efficiency at a 6 μm thick nano-TiO_2 film at this

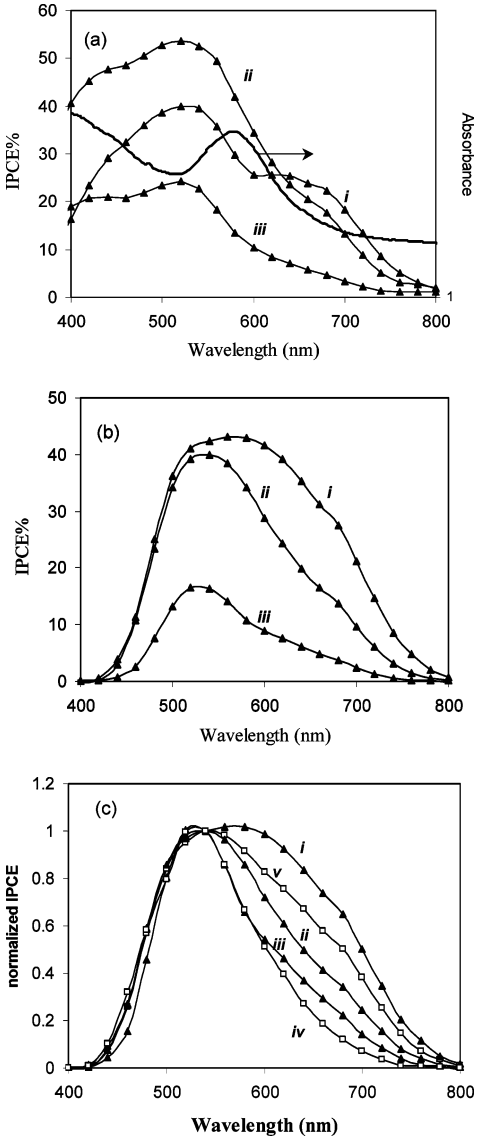

Figure 5. Photoaction spectra in back-wall (a) and front-wall illumination (b) of a dye-sensitized TiO_2 inverse opal (stop band at 580 nm)/nanocrystalline TiO_2 bilayer (i), a nanocrystalline TiO_2 film (ii), and the TiO_2 inverse opal (iii). The inverse opal film is 6 μm thick, and the TiO_2 nanocrystalline film and the bilayer structure are 10−11 μm thick. The absorbance spectrum of this photonic crystal with ethanol filling the void is presented (right axis, panel a), showing the stop band centered at 580 nm. Panel c shows normalized IPCE (front wall), with spectra iv and v corresponding respectively to the sensitized PC of the stop band at 488 nm, and the same PC coupled to a nanocrystalline TiO_2 film, presented for comparison.

wavelength, a 7% additional enhancement in IPCE at 680 nm at the bilayer can be attributed to enhancement from interfacial scattering.

When the disordered structure was subjected to a second LPD filling, the red-light conversion efficiency was increased beyond that of the original disordered film, with an enhancement factor of 2.6 at 680 nm relative to a nanoTiO_2 film of the same area (cf. Table 1). Furthermore, a significantly higher enhancement resulted when this disordered TiO_2_2 film was coupled to a nanocrystalline TiO_2 layer. This gave more than an 80% increase in the conversion efficiency in the 580−800 nm spectral range in front-wall illumination relative to a 10 μm nano-TiO_2 film (Figure 9b). In this case as well, a conversion efficiency of 12% at the 4.5 μm film at 680 nm did not account for the entire 35% IPCE at this wavelength. A synergistic effect of 15% IPCE

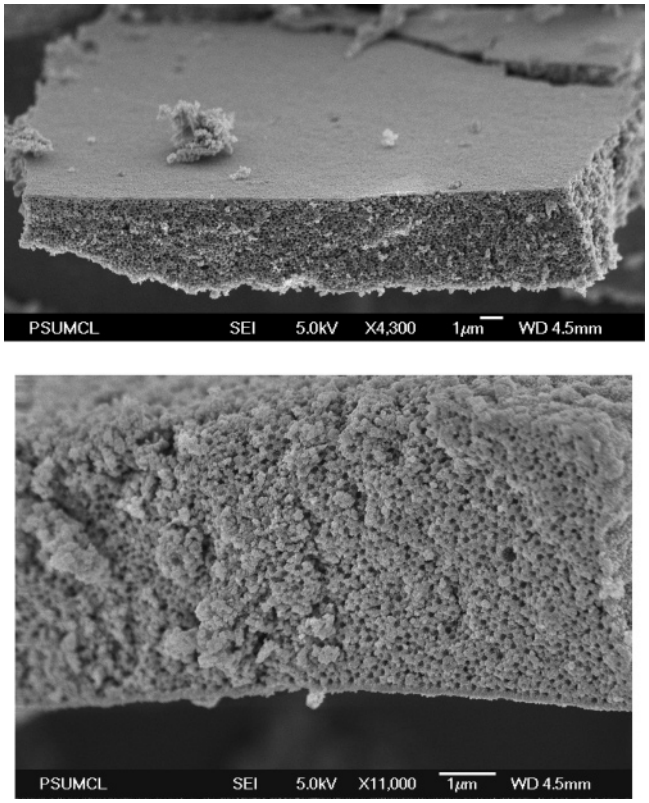

Figure 6. SEM images of a disordered TiO_2 film resulting from LPD filling of a disordered polystyrene template and calcining the spheres.

is attributed to scattering at the interface of the coupled architecture. A summary of these results comparing the gains of the different structures is presented in Tables 1 and 2.

IV. Discussion

Nanocrystalline TiO_2 films are transparent because the particles are very small (d = 10−30 nm) and the films have a high packing density. Monte Carlo simulations based on solutions of the Maxwell equation revealed that about 99% of the incident light penetrates a TiO_2 film of 30 nm particles without scattering.[10] Ferber and Luther[9] predicted that addition of larger titania particles will appreciably increase solar absorption because of enhanced multiple scattering in the film. They showed (using a numerical solution to the radiative transport equation) that adding 250−300 nm TiO_2 particles at 5 wt % to 20 nm particles results in a 27% energy gain in the solar absorption of a 10 μm film, calculated to be predominantly in the 550−750 nm spectral range where the dye extinction coefficient is low. A similar gain in light absorption was obtained for a 2 μm scattering layer of 270 nm TiO_2 particles applied onto an 8 μm nanocrystalline TiO_2 film.[9] The same approach was predicted by Usami to improve light harvesting at these films.[8] The structures studied in this work constitute geometrically similar bilayer architecture with comparable sphere size (e.g., 217 nm holes in the single LPD inverse opal), and the gain in the light conversion efficiency at long wavelengths agrees well with the theoretical prediction of enhanced absorbance as a result of scattering. Nevertheless, a marked difference is observed because of the different internal geometry of the bilayer photonic crystal TiO_2/nano-TiO_2 arrangement

With a high enough degree of scattering in disordered media, light transport is halted as a result of interference of waves that have undergone multiple scattering events, making the elastic mean free path on the order of the wavelength of light.[23−25]

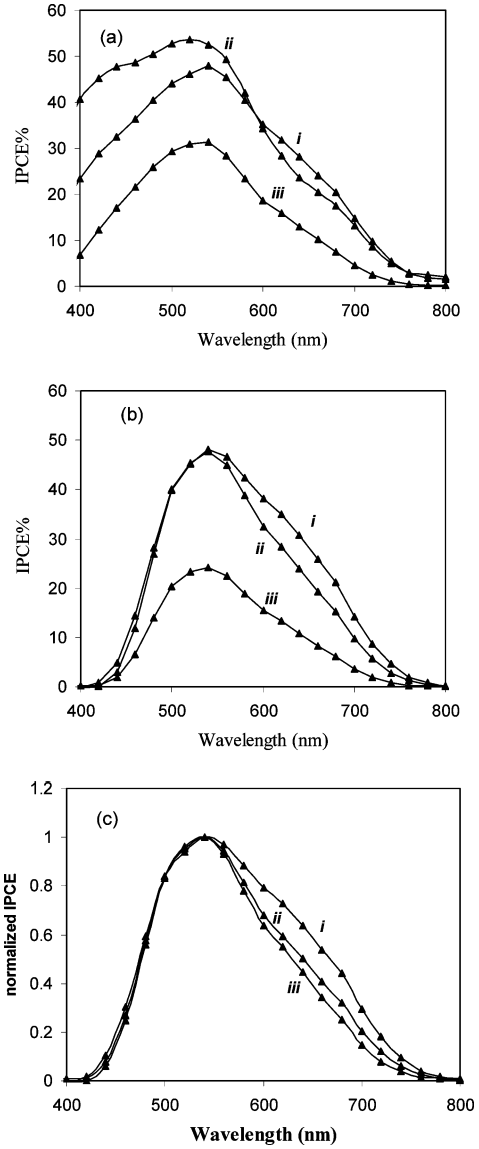

Figure 7. Photoaction spectra in back-wall (a) and front-wall illumination (b) of a dye-sensitized TiO_2 disordered inverse opal film/nanocrystalline TiO_2 bilayer (i), a nanocrystalline TiO_2 film (ii), and the disordered TiO_2 inverse opal film (iii). The TiO_2 nanocrystalline film and the bilayer structure are 10−11 μm thick. Panel c shows the IPCE (front wall) normalized at 540 nm.

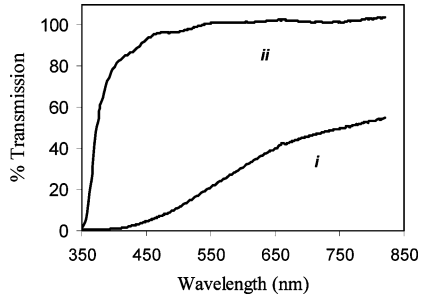

Figure 8. UV−visible transmission spectra of the disordered TiO_2 inverse opal film (i) and of a nanocrystalline TiO_2 film (ii).

This regime of strong light localization, known as Anderson localization of light,[23−25] is a phenomenon similar to the Anderson localization of electron waves,[26] which yields a transition from a conducting state to an insulating state in highly disordered semiconductors. Anderson localization of light has been reported for several systems,[27−29] such as films of highly disordered GaAs powders (e.g., 1 μm and 300 nm diameter)[28] and macroporous GaP structures.[29] It was also predicted by John that disorder at photonic crystals can lead to Anderson localization of light in these media, in what he described as a "delicate interplay between order and disorder".[30]

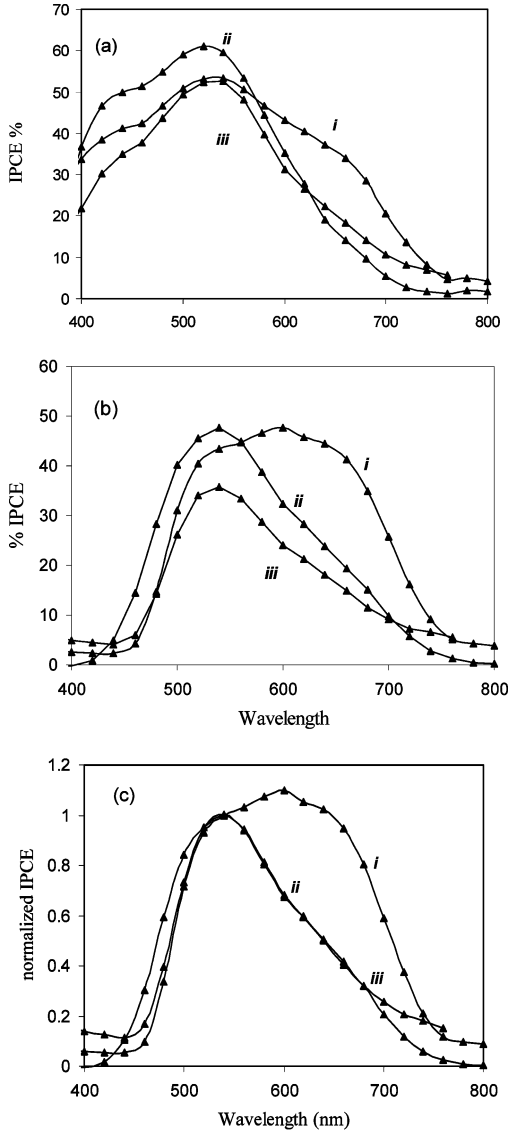

Figure 9. Photoaction spectra in back-wall (a) and front-wall illumination (b) of a dye-sensitized TiO_2 disordered inverse opal film (LPD 2)/nanocrystalline TiO_2 bilayer (i), a nanocrystalline TiO_2 film (ii), and the disordered TiO_2 _2 inverse opal film (iii). Panel c shows the IPCE (front wall) normalized at 540 nm.

Before the onset of strong localization, enhanced backscattering, also known as the weak localization regime, takes place as a result of constructive interference between counterpropagating waves in disordered media.[31−34] Disorder is common in self-assembled photonic crystals as a result of the sphere size distribution, stacking faults, and the chemical infiltration processes, and scattering can take place at these disordered regions. Koenderink et al.[35] reported enhanced backscattering from photonic crystals of polystyrene opals and air spheres in titania, with enhancement factors between 1.2 and 1.85 depending on the crystal. The backscattering cone[34] was shown to be wider at wavelengths to the red of the stop band, indicating a shorter mean free path and a higher degree of scattering, and to be narrow within the stop band from the red to the blue edge. Backcattering in this medium was modeled by diffusion theory in disordered media[31] after incorporating the effect of the photonic band.[35]

Accordingly, and in addition to Bragg diffraction by the periodic lattice, other mechanisms of light propagation in effect at photonic crystals and at disordered titania structures affect the light-conversion efficiency of these bilayer photoelectrodes. The first mechanism is the localization of light near a photonic gap, whereby light waves with wavelengths at the red edge of the stop band have higher amplitude in the medium with the higher refractive index and nodes in the medium of the low refractive index. This mechanism can be maintained in the presence of disorder in a photonic crystal, as an amorphous semiconductor retains the existence of an electronic mobility gap or pseudogaps. The second mechanism consists of multiple scattering at disordered regions in the structure; internal multiple scattering can cause an increase in the path length of light, and if the magnitude is high enough it will result in weak localization and enhanced backscattering (and ultimately in Anderson localization). Enhanced backscattering coupled with diffusely scattered background and forward scattering where present will affect the absorption of light at the coupled nanocrystalline film in the bilayer, onto which the scattered beam is directed; this will be manifested in a strong dependence on the direction of illumination.

The results of this study are interpreted on the basis of these light propagation mechanisms. At a photonic crystal with a stop band centered at 488 nm, localization of heavy photons predicted by the periodicity of the refractive index does not extend to wavelengths of 600−800 nm where absorption of the dye molecule is low. When this photonic crystal is coupled to a nano-TiO_2 film, Bragg diffraction results in a decrease in the IPCE in back-wall illumination within the photonic gap. Scattering at disordered regions in the photonic crystal enhances the intensity of light in the nano-TiO_2 film, thus increasing the conversion efficiency in the 550−800 nm spectral region in front-wall and back-wall illumination. It appears however from comparison of the spectra in Figure 4a and the normalized spectra in Figure 4c that neither backscattering nor forward scattering is particularly enhanced in this photonic crystal above diffuse scattering. Enhanced backscattering would be manifested in a higher gain in the light conversion efficiency in front-wall illumination relative to back-wall illumination. The absence of evidence for enhanced backscattering at 550−800 nm is taken as an indication of the lack of any (weak) localization that would be caused by significant internal scattering at disordered regions. This is consistent with the observation that this dye-sensitized photonic crystal electrode converts light in this spectral range at the same efficiency as a nanoTiO_2 film of identical surface area.

On the other hand, by shifting the photonic crystal stop band to 582 nm, its light conversion efficiency at 600−800 nm/(molecule of adsorbed dye) increases beyond that of a nano-TiO_2 film. This is attributed in part to heavy photons localized at the edge of the 582 nm stop band, in a spectral range where the dye has a low extinction coefficient. Furthermore, to reposition the stop band, the photonic crystal was subjected to a second LPD step, which induces more disorder and causes higher internal scattering. Increased disorder is evident from the increase in the width at half-height of the photonic crystal spectral gap region and the higher degree of scattering measured in the UV−visible absorption spectra following the second LPD step (cf. Figures 4a and 5a, secondary absorbance axes). In the photonic crystal/nano-TiO_2 bilayer, the significant attenuation in the conversion efficiency in back-wall illumination relative to a nano-TiO_2 film at wavelengths falling outside the L-gap can also be attributed to significant scattering caused by a high degree of disorder. In this case, the measured IPCE gain at 680−800 nm (in back-wall illumination, beyond the small effect accounted for by internal localization at this photonic crystal) must be caused by diffusely scattered light or a degree of forward scattering enhancing the light intensity at the nano-TiO_2 layer. It follows that the higher gain at 680−800 nm in front-wall relative to back-wall illumination is a result of enhanced backscattering over the diffuse background in the crystal, enhancing the light intensity at the nano-TiO_2 layer in front-wall illumination.

Light scattering in the disordered TiO_2 film increasing the path length of light must have also caused its slightly higher conversion efficiency at 550−800 nm compared to a nano-TiO_2 film of comparable surface area (e.g., enhancement factor of 1.5 at 680 nm). When the disordered TiO_2 structure was coupled to a nanocrystalline TiO_2 film, the IPCE was lower at 450−580 nm in back-wall illumination relative to the nanocrystalline TiO_2 film, consistent with significant scattering in the disordered film. Since the higher light conversion in the long-wavelength range in back-wall illumination compared to the nano-TiO_2 electrode must be due to a degree of diffuse or forward scattering, the more pronounced attenuation in the IPCE at 450−580 nm relative to the enhancement at 580−800 nm and the higher degree of IPCE enhancement in front-wall illumination compared to back-wall illumination show that backscattering is enhanced over diffuse and forward scattering at the disordered film. This is an indication of a degree of weak light localization at this structure.

The second LPD step increases the degree of internal scattering by inducing further disorder in the structure and a change in the void size. The resulting increase in the path length of light explains the significant monochromatic IPCE of 12% at 680 nm at this sensitized photoelectrode, appreciably higher than the original disordered film, amounting to an enhancement factor of 2.6 relative to a conventional nanocrystalline electrode of the same surface area. The measured 80% higher conversion efficiency in front-wall illumination when this film was coupled to a nano-TiO_2 film relative to a nano-TiO_2 photoelectrode is attributed to significant localization of light and the resulting scattering at the interface. Furthermore, the higher enhancement in the red spectral region in front-wall compared to back-wall illumination, relative to the nano-TiO_2 electrode, is indicative of enhanced backscattering over the diffuse or forward background, a manifestation of light localization in the disordered TiO_2_2 film.

V. Conclusions

Light propagation in scattering films of titania photonic crystals or disordered scattering titania inverse opal structures was exploited to increase the light conversion efficiency of dye-sensitized nanocrystalline TiO_2 solar cells. Higher conversion efficiency in the spectral range of 600−800 nm where the $RuL_2(SCN)_2$ dye has a low extinction coefficient was observed at disordered titania structures and inverse opals with properly positioned stop bands, and at bilayer electrodes of photonic crystals and disordered layers coupled to nanocrystalline TiO_2 films. Multiple scattering events at disordered regions in the ordered and disordered inverse opals, and to a lesser extent localization of heavy photons at the edges of a photonic gap, account for the improved light-harvesting behavior of these structures. This approach provides an alternative to re-design of the sensitizer as a means of increasing the efficiency of dye-sensitized nanocrystalline TiO_2 cells. The possibility of achieving a stronger localization of light in thicker titania photonic

crystals with different degrees of disorder, and in thicker disordered titania structures, and the resulting effect of light localization on energy conversion at such dye-sensitized electrodes are currently under investigation.

Acknowledgment. This research was supported by the NSF Center for Nanoscale Science, Grant No. DMR-0080019. L.I.H. acknowledges support from a Fulbright fellowship and from a William and Flora Hewlett grant for research leave. We thank Dr. Jinguo Wang at the Materials Research Institute (MRI) at Penn State University for acquiring the HRTEM images. We also thank Mr. Kito Holliday and Prof. Vincent Crespi for helpful discussions on scattering in disordered media.

References and Notes

(1) O'Regan, B.; Grätzel, M. *Nature* **1991**, *353*, 737.

(2) Nazeerudin, M. K.; Kay, A.; Rodicio, I.; Humphry Backer, R.; Mueller, E.; Liska, P.; Vlachopoulos, N.; Grätzel, M. *J. Am. Chem. Soc.* **1993**, *115*, 6382.

(3) (a) Barbé, C. J.; Arendse, F.; Comte, P.; Jirousek, M.; Lenzmann, F.; Shklover, V.; Grätzel, M. *J. Am. Chem. Soc.* **1997**, *80*, 33157. (b) Kalyanasundaram, K.; Grätzel, M. *Coord. Chem. Rev.* **1998**, *77*, 347.

(4) Park, N.-G.; van de Lagemaat, J.; Frank, A. J. *J. Phys. Chem. B* **2000**, *104*, 8989.

(5) (a) Huang, S. Y.; Schlichthörl, G.; Nozik, A. J.; Grätzel, M.; Frank, A. J. *J. Phys. Chem. B* **1997**, *101*, 2576. (b) Schlichthörl, G.; Huang, S. Y.; Sprague, J.; Frank, A. J. *J. Phys. Chem. B* **1997**, *101*, 8141.

(6) Stanley, A.; Matthews, D. *Aust. J. Chem.* **1995**, *48*, 1294.

(7) Tachibana, Y.; Hara, K.; Sayama, K.; Arakawa, H. *Chem. Mater.* **2002**, *14*, 2527.

(8) Usami, A. *Chem. Phys. Lett.* **1997**, *277*, 105.

(9) Ferber, J.; Luther, J. *Solar Energy Mater. Solar Cells* **1998**, *54*, 265.

(10) Usami, A. *Solar Energy Mater. Solar Cells* **1999**, *59*, 163.

(11) Rothenberger, G.; Comte, P.; Grätzel, M. *Solar Energy Mater. Solar Cells* **1999**, *58*, 321.

(12) Nishimura, S.; Abrams, N.; Lewis, B. A.; Halaoui, L. I.; Mallouk, T. E.; Benkstein, K. D.; van de Lagemaat, J.; Frank, A. J. *J. Am. Chem. Soc.* **2003**, *125*, 6306.

(13) Tocci, M. D.; Scalora, M.; Bloemer, M. J.; Dowling, J. P.; Bowden, C. W. *Phys. Rev. A* **1996**, *53*, 2799.

(14) (a) Scalora, M.; Dowling, J. P.; Bowden C. W.; Bloemer M. J. *Phys. Rev. Lett.* **1994**, *73*, 1368. (b) Dowling, J. P.; Scalora, M.; Bloemer, M. J.; Bowden, C. W. *J. Mod. Opt.* **1994**, *42*, 345. (c) Dowling, J. P.; Scalora, M.; Bloemer, M. J.; Bowden, C. W. *J. Appl. Phys.* **1994**, *75*, 1896.

(15) Vlasov, Y. A.; Petit, S.; Klein, G.; Hönerlage, B.; Hirlimann, Ch. *Phys. Rev. E* **1999**, *60*, 1030.

(16) (a) Carlson, R. J.; Asher, S. A. *Appl. Spectrosc.* **1984**, *38*, 297. (b) Flaugh, P. L.; O'Donnell, S. E.; Asher, S. A. *Appl. Spectrosc.* **1984**, *38*, 847.

(17) Wang, W.; Asher, S. A. *J. Am. Chem. Soc.* **2001**, *123*, 12528.

(18) Kang, M.; Park, Y. J.; Ryu, K. S.; Chang, S. H. *Solar Energy Mater. Solar Cells C* **2003**, *75*, 475.

(19) Nishimura, S.; Shishido, A.; Abrams, N.; Mallouk, T. E. *Appl. Phys. Lett.* **2002**, *81*, 4532.

(20) Kishimoto, H.; Takahama, K.; Hashimoto, N.; Aoi, Y.; Deki, S. *J. Mater. Chem.* **1998**, *8*, 2019.

(21) Jiang, P.; Bertone, J. F.; Hwang, K. S.; Colvin, V. L. *Chem. Mater.* **1999**, *11*, 2132.

(22) Variations in IPCE at photonic crystal structures were 10−20% within one standard deviation of the mean value at different wavelengths, while the IPCE at nano-TiO_2 photoelectrodes varied by 7−10% within one standard deviation of the mean.

(23) John, S. *Phys. Rev. Lett.* **1984**, *53*, 2169.

(24) Soukoulis, C. M.; Economou, E. N.; Grest, G. S.; Cohen, M. H. *Phys. Rev. Lett.* **1989**, *62*, 575.

(25) (a) Garcia, N.; Genack, A. Z. *Phys. Rev. Lett.* **1991**, *66*, 1850. (b) Genack, A. Z.; Garcia, N. *Phys. Rev. Lett.* **1991**, *66*, 2064.

(26) Anderson, P. W. *Phys. Rev.* **1958**, *109*, 1492.

(27) Stoytchev, M.; Genack, A. Z. *Phys. Rev. B* **1997**, 55, R8617

(28) Wiersma, D. S.; Bartolini, P.; Lagendijk, A.; Righini, R. *Nature* **1997**, *390*, 671.

(29) Schuurmans, F. J. P.; Megens, M.; Vanmaekelbergh, D.; Lagendjik, A. *Phys. Rev. Lett.* **1999**, *83*, 2183.

(30) John, S. *Phys. Rev. Lett.* **1987**, *58*, 2486.

(31) van der Mark, M. B.; van Albada, M. P.; Lagendijk, A. *Phys. Rev. B* **1988**, *37*, 3575.

(32) Wolf, P.-E.; Maret, G. *Phys. Rev. Lett.* **1985**, *55*, 2696.

(33) Albada, M. P.; Lagendijk, A. *Phys. Rev. Lett.* **1985**, 2692.

(34) To study localization of light in disordered media, the backscattered intensity can be measured as a function of the angle above the diffuse background, and the width of the cone exhibiting a maximum in the backscatter direction is taken as a measure of the degree of localization, the width being inversely proportional to the transport mean free path.[31−33]

(35) Koenderink, A. F.; Megens, M.; van Soest, G.; Vos, W. L.; Legendijk, A. *Phys. Lett. A* **2000**, *268*, 104.